CHAPTER 2

Real-time dispatch in power systems with high shares of renewable energy

Kevin Steven Morgado Gómez[1]
Andrés Felipe Duque Montenegro[2]
Universidad Nacional del Colombia, Bogotá, Colombia
Felipe Valencia Arroyave[3]
Universidad Nacional del Colombia, Medellín, Colombia
Universidad Austral de Chile, Chile
Ricardo Bolaños[4]
XM SA ESP, Colombia

Introduction

In the development of the daily scheduling process of generation plants, known as Unit Commitment, the effects associated with considering the uncertainty of the factors of the electrical network and generation in the energy dispatch process have been identified, which directly affect the possibilities of occurrence of some contingency. For this reason, predictions have been used to arrive at a reference value in variables associated with the dispatch process such as the generation associated with non-conventional renewable energies and forecasts associated with the demand for energy in different intervals (Chen *et al.*, 2014; Zhao and Guan, 2013). However, this information presents a degree of uncertainty, which depends on the quality of the reference data and the time horizon that is being evaluated.

1 ksmorgadog@unal.edu.co
2 afduquem@unal.edu.co
3 felipe.valencia@gmail.com, felipe.valencia@uach.cl
4 rabolanos@xm.com.co

For this reason, this chapter presents the implementation of a Unit Commitment modeling with uncertainty. This system was modeled using the Python Pyomo library, thermal where the IEEE 39 nodes test case was used, consisting of hydraulic and generation in conjunction with 2 renewable energy plants, whose base parameters were adapted from the actual case of the Colombian system. The latter was done to evaluate the scalability of the optimization method.

The optimization model is based on the scheduled generation dispatch to cover the expected demand in a time window of up to 24 hours so that the lowest-priced resources are used for each hour, complying with its limit conditions. The system such as rolling reserve requirements, inflexibilities, and restrictions. The main variables in the operation of the Colombian electricity system operated by XM are (XM, 2021):

- Price offers: generating companies must report daily to the NDC before 08:00 hours a single price offer to the Energy Exchange for twenty-four (24) hours (expressed in integer values $/MWh) per each generation plant for the following day.
- Availability of a generator: generating companies must report daily to the NDC before 08:00 hours the maximum amount of hourly energy (expressed as an integer value in MWh) that a generator can supply to the system during the interval of determining time.
- Configuration of ramps: daily, at the same time that they make the price offer to the Energy Exchange, they must inform the fuel and the configuration with which each generation plant must be considered in the dispatch.
- Declaration of mandatory minimums: the generation resources authorized to declare mandatory minimum generation in the daily offer, either due to technical limitations or environmental obligations, make the offer within the times established.
- AGC availability: the eligible generation plants and/or units may freely bid their availability for each day and time period to provide the secondary frequency regulation service.

A 12-buses system inspired by the Colombian power system was used to implement the proposed stochastic unit commitment and economic dispatch for exemplification purposes. In contrast, the IEEE 39-buses system was used for the same goal in the case of the proposed robust unit commitment and economic dispatch.

Nomenclature

Index and sets

$f \in \mathcal{F}^i$	Steps of the marginal cost function of unit i
$i \in I$	Generating units
$i \in I^{\mathcal{TH}}$	Thermal generating units
$i \in I^{\mathcal{HY}}$	Hydroelectric generating units
$i \in I^{\mathcal{LS}}$	Long-start generating units with $I^{\mathcal{LS}} \subseteq I^{TH}$

$j \in \mathcal{J}$	Unit start-up types $\mathcal{J} = \{h, w, c\}(=, hot, warm, cold)$
$l \in \mathcal{L}$	Loads
$m \in \mathcal{M}$	Reserves types $\mathcal{M} = \{1+, 1-, 2+, 2-, 3S, 3NS\}$, where $m = 1+$: primary-up; $m = 1-$: primary-down, $m = 2+$: secondary-up; $m = 2-$: secondary-down; $m = 3S$: tertiary spinning, $m = 3NS$ tertiary non-spinning
$\tilde{t} \in \tilde{\mathcal{T}}$	Hours
$t, \tau \in \mathcal{T}$	Time intervals (of variable duration)
$t \in \mathcal{T}^{-}$	Time intervals extended to the past
$t \in \mathcal{T}^{+}$	Time intervals extended to the future
$w \in \mathcal{W}$	Wind farms
$ph \in \mathcal{PH}$	Photovoltaic plants
$\phi \in \Phi$	Unit operating phases $\Phi = \{syn, soak, disp, des\}$ where *syn*: synchronization; *soak*: soak; *disp*: dispatchable; *des*: desynchronization
$n \in \mathcal{N}$	Number of busbars of the power system
$n \in \mathcal{N}^{\mathcal{REF}}$	Swing busbar
$n \in \mathcal{N}^{\mathcal{GEN}}$	Location of the generation units within the network
$n \in \mathcal{N}^{\mathcal{DEM}}$	Location of the load centers within the network
$row, col \in \mathbb{R}^{1\times N}$	List of from-to pairs for the construction of the impedance/ admittance network matrix
$s \in \mathcal{S}$	Scenarios considered in the stochastic programming approach

Parameters

$B_{i,f,t}$	Size of step f of unit i marginal cost function, during time interval t, in MW
$C_{i,f,t}$	Marginal cost of step f of unit i marginal cost function, during time interval t, in COP
h_t	Duration of time interval t, in h
NLC_i	No-load cost of unit i, in \$/h
$P_i^{\max(\min)}$	Maximum (minimum) active power output of unit i, in MW
$P_i^{\max,AGC}$	Maximum power output of unit i while operating in AGC, in MW
$P_i^{\min,AGC}$	Minimum power output of unit i while operating in AGC, in MW
$P_{i,\tau,t}^{soak,j}$	Power output of unit i, at soak phase, during time interval t, after a j-type start-up that initiates at time interval τ, in MW
$P_{i,\tau,t}^{des}$	Power output of unit i, at desynchronization phase, during time interval t, before the respective shut-down that occurs at the time interval τ, in MW
$P_{l,t}$	Effective load l during time interval t, in MW
$P_{w,t}$	Available wind power in wind farm w, during the time interval t, in MW

$P_{ph,t}$	Available photovoltaic power in photovoltaic plant *ph*, during the time interval *t*, in MW
$R_i^{\max,m}$	Maximum contribution (ramp limited) of unit *i*, in reserve type *m*, in MW
RD_i	Ramp-down rate of unit *i*, in MW/min
$R_t^{sys,m}$	System requirement in reserve type *m*, time interval *t*, in MW
$S_{k,n,t}^{\max}$	Line capacity at time t, in MVAR
RU_i	Ramp-up rate of unit *i*, in MW/min
SDC_i	Shut-down cost of unit *i*, in COP
SUC_i^j	Start-up cost of unit *i*, from start-up type *j* until load with synchronization, in COP
T	Number of time intervals of the operation horizon
$T_{i,t}^{up(dn)}$	Minimum up (down) time of unit *i*, at time interval *t*, in time intervals (BWL)
$T_{i,t}^{hw(wc)}$	Off-load time before going from hot (warm) standby to warm (cold) standby condition of unit *i*, at time interval *t*, in time intervals BWL
$T_{i,t}^{syn,j}$	Synchronization time of unit *i*, under start-up type *j*, at time interval *t*, in time intervals BWL
$T_{i,t}^{soak,j}$	Soak time of unit *i*, under start-up type *j*, at time interval *t*, in time intervals BWL
$T_{i,t}^{des}$	Desynchronization time of unit *i*, under start-up type *j*, at time interval *t*, in time intervals BWL
$Q_i^{\max(\min)}$	Maximum (minimum) reactive power output of unit *i*, in MVAR
$Y_{row,col}$	Admittance matrix of the power system
p^s	Probability of occurrence of scenario *s*

Variables

$\alpha_{w,t}$	Percentage of dispatched wind power of wind farm *w*, at time interval *t*, in %
$\alpha_{ph,t}$	Percentage of dispatched photovoltaic power of photovoltaic plant *ph*, at time interval *t*, in %
$\beta_{i,f,t}$	Portion of step *f* of the *i*-th unit marginal cost function loaded in time interval *t*, in p.u.
$p_{i,t}$	Active power output of unit *i*, during the time interval *t*, in MW
$p_{i,t}^{des(soak)}$	Power output of unit *i* during the desynchronization (soak) phase, at time interval *t*, in MW
$p_{w,t}$	Power output of wind farm *w*, at time interval *t*, in MW
$p_{ph,t}$	Power output of photovoltaic plant *ph*, at time interval *t*, in MW
$r_{i,t}^m$	Contribution of unit *i* in reserve type *m*, during the time interval *t*, in MW

$u_{i,t}$	Binary variable which is equal to 1 if unit i is on
$u_{i,t}^{\phi}$	Binary variable which is equal to 1 if unit i is in operating phase ϕ, during time interval t
$u_{i,t}^{AGC}$	Binary variable which is equal to 1 if unit i provides secondary reserve during time interval t
$u_{i,t}^{3NS}$	Binary variable which is equal to 1 if unit i provides tertiary non-spinning reserve during time interval t
$y_{i,t}$	Binary variable which is equal to 1 if unit i is started-up during time interval t
$y_{i,t}^{j}$	Binary variable which is equal to 1 if a tupe-j start-up of unit i is initiated during time interval t
$z_{i,t}$	Binary variable which is equal to 1 if unit i is shut-down during time interval t
$p_{n,t}^{SCH}$	Active power injected to the system at busbar n during the interval t, in MW
$q_{n,t}^{SCH}$	Reactive power injected (demanded) to (from) the system at busbar n during the interval t, in MVAR
$q_{i,t}$	Reactive power output of unit i, during the time interval t, in MVAR
$sl_{row,col,t}$	Power flowing through the transmission lines and transformers (row, col), during the time interval t, in MVA

Uncertainty representation

The selection of the uncertainty set influences the formulation of the model to be implemented. There are different alternatives to represent uncertainty. The most common are uncertainty sets, decision trees, and possible scenarios/realizations of the uncertain variables. Below are some of the main sets taken into account in the literature according to Li and Floudas (n.d.), and the graphical representation of 2 of them is shown in figure 1.

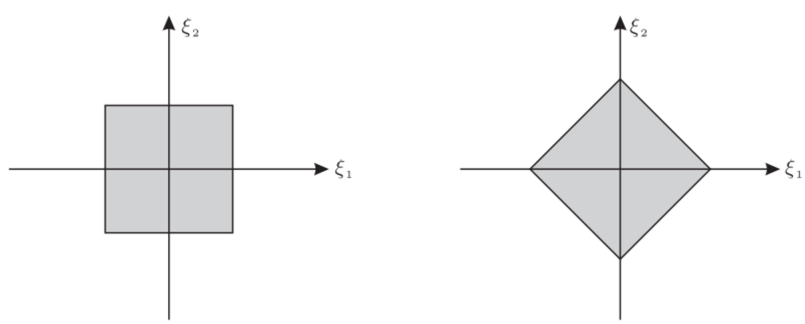

Figure 1. Set of box uncertainty (left) and polyhedron uncertainty (right)

Source: Babazadeh and Torabi (2018).

Box uncertainty set

$$U_\infty = \{\xi \mid \quad ||\xi||_\infty \leq \Psi\} = \{\xi| \quad |\xi_j| \leq \Psi, \forall j \in J_i\} \tag{1}$$

Ellipsoid uncertainty set

$$U_2 = \{\xi| \quad ||\xi||_2 \leq \Omega\} = \left\{\xi \left| \sum_{j\in J_i} \xi_j^2 \leq \Omega^2 \right.\right\} \tag{2}$$

Polyhedron uncertainty set

$$U_1 = \{\xi| \quad ||\xi|| \leq \Gamma\} = \left\{\xi \left| \sum_{j\in J_i} |\xi_j| \leq \Gamma \right.\right\} \tag{3}$$

An example of ensemble uncertainty modeling in the field of power systems is shown by An and Zeng (2015), where the uncertainty associated with the load of a power system was modeled from the so-called uncertainty constraint budget, taking into account a hypercubic set defined by the equation 4.

$$U = \left\{u_t : u_t \in [\overline{u}_t - \widehat{u}_t, \overline{u}_t + \widehat{u}_t], \sum_t \frac{|u_t - \overline{u}_t|}{\widehat{u}_t} \leq \Gamma\right\} \tag{4}$$

Γ represents the probability that u_t takes the value of the lower or upper bounds. About this system, Lorca and Sun (2015) describe what are called static uncertainty sets, in which the uncertainties of future time periods are unrelated to previous periods. An example of this set, taking into account the net demand uncertainty $\mathbf{d}_t = (d_{1t}, \ldots, d_{N^d t})$, is shown in the equation 5.

$$D_t = \left\{\mathbf{d}_t : \sum_{j\in\mathcal{N}^d} \frac{|d_{jt} - \overline{d}_{jt}|}{\widehat{d}_{jt}} \leq \Gamma^d \sqrt{N^d}, d_{jt} \in [\overline{d}_{jt} - \Gamma^d \widehat{d}_{jt}, \overline{d}_{jt} + \Gamma^d \widehat{d}_{jt}] \quad \forall j \in \mathcal{N}^d\right\} \tag{5}$$

where $\mathcal{N}^d, N^d$ represent the set and number of loads respectively and with d_{jt} being the net demand for load j in time t. In this distribution, d_{jt} is located in an interval centered on a reference value $\overline{d}_{jt}$ with a width determined by the deviation $\widehat{d}_{jt}$. In turn, as in the previous case, Γ controls the size of the uncertainty. It protects the robust solution against variations in demand (Lorca and Sun, 2015).

On the other hand, the development of dynamic sets has been proposed to explicitly model the correlation between multiple uncertainty resources in a time interval, defined by the equation 6.

$$\Xi_t(\xi_{[1:t-1]}) = \{\xi_t : \exists \mathbf{u}_{[t]} \quad \text{s.t.} \quad f(\xi_{[t]}, \mathbf{u}_{[t]}) \leq 0\} \tag{6}$$

In this equation, the uncertainty vector ξ_t depends on the vector of convex functions defined by $f(\xi_{[t]}, \mathbf{u}_{[t]})$, the latter being semi-defined and representable. Based on this, research has been developed such as the one presented by Zhao and Zeng (2012), in which the modeling of uncertainties associated with forms of renewable generation has been sought, in this case, the definition of polyhedrons formed from constraints of edge and multiple budget uncertainty constraints (Zhao and Zeng, 2012).

$$V = \left\{ \underline{v}_t \le v_t \le \bar{v}_t, \sum_{t \in T_1} \theta_t v_t \ge V_1^{\prime}, \sum_{t \in T_2} \theta_t v_t \ge V_2^{\prime}, \ldots, \sum_{t \in T_{seg}} \theta_t v_t \ge V_{seg}^{\prime} \right\} \qquad (7)$$

Contrary to uncertainty sets, constructing decision trees or scenarios requires defining the decision stages to be considered in the model or defining those special cases to be analyzed.

In the first case, the unit commitment problem is divided into 2 stages: turning the units on and off and defining the power generation schedule. It should be noted that the decisions to switch on and off cannot be altered once the uncertainty has manifested/materialized. Thus, each unit's generation and reserves program is adjusted for each scenario to satisfy the system's physical and operating restrictions.

In the second case, the cases/circumstances are defined depending on the projections or level of security it desires against the materialization of the uncertainty. An alternative is shown below:

1. Circumstance 1: low demand, low solar generation, and low wind generation.
2. Circumstance 2: low demand, high solar generation, and high wind generation (lower bound expected dispatch cost).
3. Circumstance 3: average demand, average solar generation, and average wind generation.
4. Circumstance 4: medium demand, high solar generation, and low wind generation.
5. Circumstance 5: high demand, low solar generation, and low wind generation (Upper bound expected dispatch cost.)
6. Circumstance 6: high demand, high solar generation, and high wind generation.

A unit commitment was implemented in the research carried out in Du *et al.* (2019). The uncertainty was modeled through scenarios or sequences of possible values for the uncertain variables, particularly solar radiation. Figure 2 presents the scenarios analyzed, their probability of occurrence, and the decision tree that gives rise to each system.

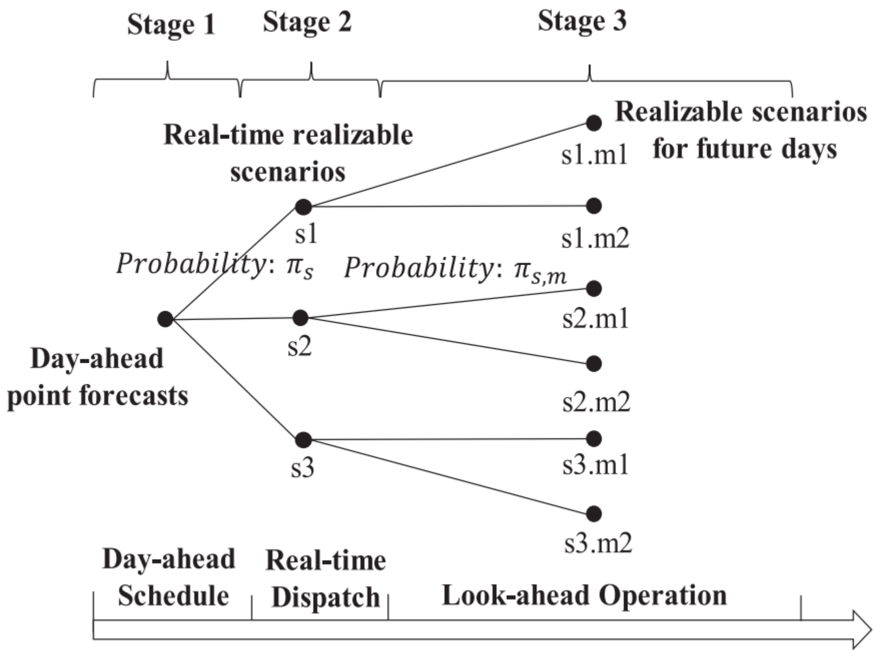

Figure 2. Uncertainty representation in a 3-stage scenario

Source: Du *et al.* (2019).

Unit commitment formulation for the short-term operation of power systems

Consider the unit commitment formulation presented by Bakirtzis *et al.* (2014a):

$$\min \sum_{t \in T} \sum_{i \in I} \left(h_t \left(\sum_{f \in \mathcal{F}^i} (C_{i,f,t} B_{i,f,t} \beta_{i,f,t}) + \mathrm{NLC}_i (u_{i,t} - u_{i,t}^{syn}) \right) + \sum_{j \in \mathcal{J}} \mathrm{SUC}_t^j y_{i,t}^j + \mathrm{SDC}_i z_{i,t} \right) \quad (8)$$

Subject to

$$u_{i,\tilde{t}} \geq \sum_{\tilde{\tau} = \tilde{t} - \tilde{T}_i^{up} + 1}^{\tilde{t}} y_{i,\tilde{\tau}} \quad \forall \tilde{t} \in \widetilde{\mathcal{T}} \quad (9)$$

$$u_{i,t} \geq \sum_{\tau = t - T_i^{up} + 1}^{t} y_{i,\tau} \quad \forall t \in \mathcal{T} \quad (10)$$

$$P^{soak,j}_{i,\tau,t} = P^{\min}_i \frac{\left(\sum_{t=\tau+T^{syn*,j}_{i,\tau}}^{t} h_t\right)}{\left(\sum_{t=\tau+T^{syn*,j}_{i,\tau}}^{\tau+T^{syn*,j}_{i,\tau}+T^{soak*,j}_{i,\tau+T^{syn*,j}_{i,\tau}}-1} h_t\right)} \quad \forall i \in I^{\mathcal{TH}}, \tau \in \mathcal{T}^{-} \tag{11}$$

$$\tau + T^{syn*,j}_{i,t} \leq t \leq \tau + T^{syn*,j}_{i,t} + T^{soak*,j}_{i,\tau+T^{syn*,j}_{i,\tau}} - 1 \tag{12}$$

$$P^{soak,j}_{i,\tau,j} = 0 \quad \text{otherwise} \tag{13}$$

$$P^{des,j}_{i,\tau,t} = P^{\min}_i \frac{\left(\sum_{t=t}^{\tau-1} h_t\right)}{\left(\sum_{t=\tau-T^{des}_{i,\tau}}^{\tau-1} h_t\right)} \quad \forall i \in T^{TH}, \tau \in T^{+}, \tau - T^{des}_{i,\tau} \leq t \leq \tau - 1 \tag{14}$$

$$P^{des}_{i,\tau,t} = 0 \quad \text{otherwise} \tag{15}$$

$$u_{i,t} = u^{syn}_{i,t} + u^{soak}_{i,t} + u^{disp}_{i,t} + u^{des}_{i,t} \quad \forall i \in I, t \in \mathcal{T} \tag{16}$$

$$y_{i,t} - z_{i,t} = u_{i,t} - u_{i,t-1} \quad \forall i \in I, t \in \mathcal{T} \tag{17}$$

$$y_{i,t} + z_{i,t} \leq 1 \quad \forall i \in I, t \in \mathcal{T} \tag{18}$$

$$y_{i,t} = \sum_{j \in \mathcal{J}} y^{j}_{i,t} \quad \forall i \in I^{\mathcal{TH}}, t \in \mathcal{T} \tag{19}$$

$$y^{h}_{i,t} \leq \sum_{\tau=t-T^{hw}_{i,t}+1} z_{i,t} \quad \forall i \in I^{\mathcal{TH}}, t \in \mathcal{T} \tag{20}$$

$$y^{w}_{i,t} \leq \sum_{\tau=t-T^{wc}_{i,t}+1}^{t-T^{hw}_{i,t}} z_{i,t} \quad \forall i \in I^{\mathcal{TH}}, t \in \mathcal{T} \tag{21}$$

$$y^{c}_{i,t} \leq \sum_{\tau=1}^{t-T^{wc}_{i,t}} z_{i,t} \quad \forall i \in I^{\mathcal{TH}}, t \in \mathcal{T} \tag{22}$$

$$u^{syn}_{i,t} = \sum_{j \in \mathcal{J}} \left(\sum_{t-T^{syn,j}_{i,t}+1}^{t} y^{j}_{i,\tau} \right) \quad \forall i \in I^{\mathcal{TH}}, t \in \mathcal{T} \tag{23}$$

$$u^{soak}_{i,t} = \sum_{j \in \mathcal{J}} \left(\sum_{t-T^{soak,j}_{i,t}-T^{syn,j}_{i,t-T^{soak,j}_{i,t}}+1}^{t} y^{j}_{i,\tau} \right) \quad \forall i \in I^{\mathcal{TH}}, t \in \mathcal{T} \tag{24}$$

$$p^{soak}_{i,t} = \sum_{j \in \mathcal{J}} \left(\sum_{t-T^{soak,j}_{i,t}-T^{syn,j}_{i,t-T^{soak,j}_{i,t}}+1}^{t-T^{syn,j}_{i,t}} y^{j}_{i,\tau} P^{soak,j}_{i,\tau,t} \right) \quad \forall i \in I^{\mathcal{TH}}, t \in \mathcal{T} \tag{25}$$

$$u_{i,t}^{des} = \sum_{\tau=t+1}^{t+T_{i,t+1}^{des^*}} z_{i,\tau} \quad \forall i \in I^{\mathcal{TH}}, t \in \mathcal{T} \tag{26}$$

$$p_{i,t}^{des} = \sum_{\tau=t+1}^{t+T_{i,t+1}^{des^*}} z_{i,\tau} \cdot P_{i,\tau,t}^{des} \quad \forall i \in I^{TH}, t \in T \tag{27}$$

$$u_{i,t} \geq \sum_{\tau=t-T_{i,t}^{up}+1}^{t} y_{i,\tau} \quad \forall i \in I^{\mathcal{TH}}, t \in T \tag{28}$$

$$1 - u_{i,t} \geq \sum_{\tau=t-T_{i,t}^{dn}+1}^{t} z_{i,\tau} \quad \forall i \in I^{\mathcal{TH}}, t \in T \tag{29}$$

$$p_{i,t} - p_{i,t-1} \leq RU_i h_{t-1} + P_i^{\max}(y_{i,t} + u_{i,t}^{syn} + u_{i,t}^{soak}) \quad \forall i \in I, t \in \mathcal{T} \tag{30}$$

$$p_{i,t-1} - p_{i,t} \leq RD_i h_{t-1} + P_i^{\max}(u_{i,t-1}^{des} + z_{i,t}) \quad \forall i \in I, t \in \mathcal{T} \tag{31}$$

$$p_{i,t} + r_{i,t}^{1+} + r_{i,t}^{2+} + r_{i,t}^{3S} \leq 0(u_{i,t}^{syn}) + p_{i,t}^{soak} + p_{i,t}^{des} + P_i^{\max} u_{i,t}^{disp} \quad \forall i \in I, t \in \mathcal{T} \tag{32}$$

$$p_{i,t} - r_{i,t}^{1-} - r_{i,t}^{2-} \geq 0(u_{i,t}^{syn}) + p_{i,t}^{soak} + p_{i,t}^{des} + P_i^{\min} u_{i,t}^{disp} \quad \forall i \in I, t \in T \in \mathcal{T} \tag{33}$$

$$\begin{aligned} p_{i,t} + r_{i,t}^{2+} \leq\ & 0(u_{i,t}^{syn}) + p_{i,t}^{soak} + p_{i,t}^{des} + P_i^{\max}(u_{i,t}^{disp} - u_{i,t}^{AGC}) \\ & + P_i^{\max,AGC} u_{i,t}^{AGC} \quad \forall i \in I, t \in T \end{aligned} \tag{34}$$

$$\begin{aligned} p_{i,t} - r_{i,t}^{2-} \leq\ & 0(u_{i,t}^{syn}) + p_{i,t}^{soak} + p_{i,t}^{des} + P_i^{\min}(u_{i,t}^{disp} - u_{i,t}^{AGC}) \\ & + P_i^{\min,AGC} u_{i,t}^{AGC} \quad \forall i \in I, t \in \mathcal{T} \end{aligned} \tag{35}$$

$$p_{i,t} + r_{i,t}^{1+} + r_{i,t}^{1-} + r_{i,t}^{2+} + r_{i,t}^{2-} + r_{i,t}^{3S} + r_{i,t}^{3NS} \leq P_i^{\max} \quad \forall i \in I, t \in \mathcal{T} \tag{36}$$

$$u_{i,t}^{AGC} \leq u_{i,t}^{disp} \quad \forall i \in I, t \in T \tag{37}$$

$$0 \leq r_{i,t}^{m} \leq R_i^{\max,m} \cdot u_{i,t}^{disp} \quad \forall i \in I, t \in T, m \in \{1+, 1-, 3S\} \tag{38}$$

$$0 \leq r_{i,t}^{m} \leq R_i^{\max,m} \cdot u_{i,t}^{AGC} \quad \forall i \in I, t \in \mathcal{T}, m \in \{2^+, 2^-\} \tag{39}$$

$$0 \leq r_{i,t}^{m} \leq R_i^{\max,m} \cdot u_{i,t}^{3NS} \quad \forall i \in I, t \in \mathcal{T}, m \in \{3NS\} \tag{40}$$

$$P_i^{\min} \cdot u_{i,t}^{3NS} \leq r_{i,t}^{3NS} \leq R_i^{\max,3NS} \cdot u_{i,t}^{3NS} \quad \forall i \in I, t \in T \tag{41}$$

$$u_{i,t}^{3NS} \leq 1 - u_{i,t} \quad \forall i \in I, t \in \mathcal{T} \tag{42}$$

$$\sum_{i \in \mathcal{I}} r_{i,t}^{m} \geq R_t^{sys,m} \quad \forall t \in \mathcal{T}, m \in \{1^+, 1^-, 2^+, 2^-\} \tag{43}$$

$$\sum_{i \in \mathcal{I}} r_{i,t}^{3S} + \sum_{i \in I} r_{i,t}^{3NS} \geq R_t^{sys,3} \quad \forall t \in \mathcal{T} \tag{44}$$

$$\sum_{i \in \mathcal{I}} p_{i,t} + \sum_{w \in \mathcal{W}} p_{w,t} + \sum_{ph \in \mathcal{PH}} p_{ph,t} = \sum_{l \in L} p_{l,t} \quad \forall t \in \mathcal{T}, \forall \tag{45}$$

$$p_{i,t} \leq P_{i,t} \quad \forall t \in \mathcal{T}, i \in \mathcal{I} \tag{46}$$

$$p_{w,t} \leq \alpha_{w,t} \cdot P_{w,t} \quad \forall t \in T, w \in \mathcal{W} \tag{47}$$

$$p_{ph,t} \leq \alpha_{ph,t} \cdot P_{ph,t} \quad \forall t \in T, ph \in \mathcal{PH} \tag{48}$$

$$\sum_{f \in \mathcal{F}^i} B_{i,f,t}\beta_{i,f,t} = p_{i,t} \quad \forall i \in \mathcal{I}, \forall t \in \mathcal{T} \tag{49}$$

$$0 \leq \beta_{i,f,t} \leq 1 \quad \forall i \in \mathcal{I}, \forall f \in \mathcal{F}i, \forall t \in \mathcal{T} \tag{50}$$

It is important to remark that, in the minimization problem (8)-(50), constraints (11)-(13) reflect the soak phase of generation units; constraints (14) and (15) reflect the power output of generation units at the desynchronization phase; constraints (19)-(22) define the type of start-up for generation units; constraints (30)-(36) define the power output limits including the reserves, whereas constraints (37)-(44) define the reserves of each generation unit, and finally constraint (45) corresponds to the power balance. Moreover, note that minimization problem (8)-(50) considers a single-node representation of the transmission network of the system. This consideration over-simplifies the system representation and could lead to unexpected/unrealizable power dispatch, even more so if it is considered the uncertainty in the load and the generation produced by integrating converter interfaced generation technologies like solar- and wind-based. Furthermore, due to the variability of these technologies, voltages at the busbars must be estimated to foresee if there will be voltage issues in the system. This could be done by integrating a more detailed transmission network model. Therefore, the convex representation of the power flow equations proposed in Jabr (2007, 2008) was included here. From this formulation, the conditions were derived to determine how loaded lines and transformers are, thus limiting the power flowing through them. Let $Y_{\text{bus}} = G + \sqrt{-1}B$ denote the admittance matrix of the system, with: G the conductance matrix and B the susceptance matrix; let $rl_{k,n} = V_k V_n \cos(\delta_k - \delta_n)$, $tl_{k,n} = V_k V_n \sin(\delta_k - \delta_n)$, and $\vartheta_k = \frac{V_k^2}{\sqrt{2}}$. Then, the power flow equations become:

$$\sqrt{2}G_{n,n}\vartheta_n + \sum_{\substack{k \in \mathcal{N}^{\mathcal{GEN}} \cup \mathcal{N}^{\mathcal{DEM}} \\ n \neq k}} \left[G_{k,n}rl_{k,n} + B_{k,n}tl_{k,n}\right] = p_n^{\text{SCH}}$$
$$\forall n \in \mathcal{N}^{\mathcal{GEN}} \cup \mathcal{N}^{\mathcal{DEM}} \tag{51}$$

$$-\sqrt{2}B_{n,n}\vartheta_n - \sum_{\substack{k \in \mathcal{N}^{\mathcal{DEM}} \\ n \neq k}} \left[B_{k,n}rl_{k,n} - G_{k,n}tl_{k,n}\right] = q_n^{\text{SCH}} \quad \forall n \in \mathcal{N}^{\mathcal{DEM}} \tag{52}$$

where p_n^{SCH} and q_n^{SCH} denote the active and reactive power injected at node n, respectively. In addition, for the definition of $rl_{k,n}$, $tl_{k,n}$, and ϑ_n, the following conditions arise:

- $rl_{k,n} = rl_{n,k}$ and $tl_{k,n} = -tl_{n,k}$ holds $\forall k, n \in \mathcal{N}$.
- $2\phi_k\phi_n = rl_{k,n}^2 + tl_{k,n}^2$ holds $\forall k, n \in \mathcal{N}$.
- $|Y_{k,n}(\phi_k - \phi_n)| \leq S_{\max,k,n}$ holds $\forall k, n \in \mathcal{N}$.

with $S_{\max,k,n}$ the power flow limit of the element connecting the nodes k and n (lines or transformers). The first condition shows the symmetry of $rl_{k,n}$ and $tl_{k,n}$, and put forward that only half of the Y_{bus} matrix must be used in the solution of the power flow equations; the second condition establishes the relationship among the decision variables $rl_{k,n}$, $tl_{k,n}$, and ϑ_n; and the third condition limits the power flowing through the elements of the system and allows deriving element (group of elements) cuts and other approximated security techniques instead of performing a security-constrained power flow within the unit commitment and power dispatch.

Finally, combining the minimization problem (8)-(50) with equations (51) and (52) and the conditions derived from them and the definitions of $rl_{k,n}$, $tl_{k,n}$, and ϑ_n, the unit commitment formulation for power system's short-term operation is obtained. Such combination yields:
min Cost Function (8)
Subject to
Constraints (9)-(50)

$$\sqrt{2}G_{n,n}\vartheta_{n,t} + \sum_{\substack{k\in\mathcal{N}^{\mathcal{GEN}}\cup\mathcal{N}^{\mathcal{DEM}}\\ n\neq k}} \left[G_{k,n}rl_{k,n,t} + B_{k,n}tl_{k,n,t}\right] = p_{n,t}^{\text{SCH}} \; \forall n \in \mathcal{N}^{\mathcal{GEN}} \cup \mathcal{N}^{\mathcal{DEM}}, \forall t \in \mathcal{T} \quad (53)$$

$$-\sqrt{2}B_{n,n}\vartheta_{n,t} - \sum_{\substack{k\in\mathcal{N}^{\mathcal{DEM}}\\ n\neq k}} \left[B_{k,n}rl_{k,n,t} - G_{k,n}tl_{k,n,t}\right] = q_{n,t}^{\text{SCH}} \; \forall n \in \mathcal{N}^{\mathcal{DEM}}, \forall t \in \mathcal{T} \quad (54)$$

$$rl_{k,n,t} = rl_{n,k,t} \;\; \forall k,n \in \mathcal{N}, \forall t \in \mathcal{T} \quad (55)$$

$$tl_{k,n,t} = -tl_{n,k,t} \;\; \forall k,n \in \mathcal{N}, \forall t \in \mathcal{T} \quad (56)$$

$$2\phi_{k,t}\phi_{n,t} = rl_{k,n,t}^2 + tl_{k,n,t}^2 \;\; \forall k,n \in \mathcal{N}, \forall t \in \mathcal{T} \quad (57)$$

$$|Y_{k,n}(\phi_{k,t} - \phi_{n,t})| \leq S_{k,n,t}^{\max} \; \forall k,n \in \mathcal{N}, \forall t \in \mathcal{T} \quad (58)$$

$$p_{n,t}^{\text{SCH}} = p_{i,t} + p_{w,t} + p_{ph,t} - p_{l,t} \;\; \forall n \in \mathcal{N}, \forall t \in \mathcal{T}, \forall i \in \mathcal{I}, \forall w \in \mathcal{W}, \forall ph \in \mathcal{PH}, \forall l \in \mathcal{L} \quad (59)$$

$$q_{n,t}^{\text{SCH}} = q_{i,t} - q_{l,t} \;\; \forall n \in \mathcal{N}, \forall t \in \mathcal{T}, \forall i \in \mathcal{I}, \forall l \in \mathcal{L} \quad (60)$$

Note that in equations (59) and (60) hold $\{\mathcal{I}, \mathcal{W}, \mathcal{PH}\} \subset \mathcal{N}^{\mathcal{GEN}}$ and $\mathcal{L} \subset \mathcal{N}^{\mathcal{DEM}}$. Furthermore, the combination of equations (8)-(50) with equations (51) and (52) and the conditions derived from them and the definitions of $rl_{k,n}$, $tl_{k,n}$, and ϑ_n define the deterministic version of the unit commitment for the short-term operation of power systems. Therefore, an uncertainty representation must be included.

Stochastic approach for the real-time operation of power systems

Let $s \in S$ denote the $s-th$ scenario/realization of the uncertain variables (generation of photovoltaic plants, generation of wind farms, and demand). Then, the deterministic formulation of the unit commitment for the short-term operation of power systems can be transformed into an expected value problem to include the uncertainty representation using scenarios. For doing this, the cost function is redefined as:

$$\min \sum_{s\in\mathcal{S}} p^{s} \sum_{t\in T} \sum_{i\in I} \left(h_t \left(\sum_{f\in\mathcal{F}^i} (C_{i,f,t}B_{i,f,t}\beta_{i,f,t}) + \mathrm{NLC}_i(u_{i,t} - u_{i,t}^{syn}) \right) + \sum_{j\in\mathcal{J}} \mathrm{SUC}_t^j y_{i,t}^j + \mathrm{SDC}_i z_{i,t} \right)^s \tag{61}$$

Moreover, the power flow equations (53) - (61) must be written as:

$$\sqrt{2}G_{n,n}\vartheta_{n,t} + \sum_{\substack{k\in\mathcal{N}^{\mathcal{GEN}}\cup\mathcal{N}^{\mathcal{DEM}}\\ n\neq k}} \left[G_{k,n}rl_{k,n,t} + B_{k,n}tl_{k,n,t}\right] = p_{n,t}^{\mathrm{SCH},s} \quad \forall n \in \mathcal{N}^{\mathcal{GEN}} \cup \mathcal{N}^{\mathcal{DEM}}, \forall t \in \mathcal{T}, \forall s \in \mathcal{S} \tag{62}$$

$$-\sqrt{2}B_{n,n}\vartheta_{n,t} - \sum_{\substack{k\in\mathcal{N}^{\mathcal{DEM}}\\ n\neq k}} \left[B_{k,n}rl_{k,n,t} - G_{k,n}tl_{k,n,t}\right] = q_{n,t}^{\mathrm{SCH},s} \quad \forall n \in \mathcal{N}^{\mathcal{DEM}}, \forall t \in \mathcal{T}, \forall s \in \mathcal{S} \tag{63}$$

where $p_{n,t}^{\mathrm{SCH},s} = p_{i,t} + p_{w,t}^{s} + p_{ph,t}^{s} - p_{l,t}^{s}$, $\forall n \in \mathcal{N}, \forall t \in \mathcal{T}, \forall i \in \mathcal{I}, \forall w \in \mathcal{W}, \forall ph \in \mathcal{PH}$, $\forall l \in \mathcal{L}, \forall s \in \mathcal{S}$; and $q_{n,t}^{\mathrm{SCH},s} = q_{i,t} - q_{l,t}^{s}$, $\forall n \in \mathcal{N}, \forall t \in \mathcal{T}, \forall l \in \mathcal{L}, \forall s \in \mathcal{S}$.

To solve stochastic programming problems, the extensive form and the progressive-hedging algorithms are often considered (Birge and Dempstert, 1996; Atakan and Sen, 2018). These alternatives are broadly selected because:

- They either take advantage of the mathematical structure of the problem (Birge and Dempstert, 1996) or use decomposition methods to reduce the computational burden of the solution (Atakan and Sen, 2018).
- They are focused on the solution of two-level stochastic programming problems that use a sample of scenarios as a proxy of the uncertain variables/parameters.

It is important to remark that using scenarios for uncertainty representation might result in massive optimization problems to provide a high-quality solution consistently. Accordingly, solving stochastic programming problems relies on decomposition methods developed to reduce their computational burden. These decompositions are either made concerning the scenarios or with the decision model's time periods (Birge and Dempstert, 1996; Atakan and Sen, 2018).

In the former, the decision variables for the second stage and the coupling non-anticipative constraints at each node in the scenario tree are explicitly described. This is called the extensive form of stochastic programming and looks to transform the original stochastic programming problem into an equivalent deterministic mix-integer problem (Bynum *et al.*, 2021; Hart *et al.*, 2011; Watson *et al.*, 2012). The advantage of this form recast is the fact that the constraints added by the scenarios/realizations of the uncertain variables/parameters have a particular structure that could be exploited through several matrix factorizations and, therefore, reduce the complexity of the equivalent deterministic optimization problem (Birge and Dempstert, 1996). Algorithms reported that using matrix factorizations to reduce the complexity of the extensive form of stochastic programming problems include the L-shaped method and the nested Benders' decomposition (for details of these algorithms and other approaches, see Birge and Dempstert, 1996; Atakan and Sen, 2018 and the references therein).

The non-anticipative constraints are dualized in the latter, and the resulting subproblems are solved independently (Atakan and Sen, 2018). This brings a high degree of parallelization to this approach and significantly reduces the computational burden of solving stochastic programming problems. However, coordinating the dual variables is not trivial; therefore, obtaining the optimal prices could be difficult. Thereby, the parameters of the progressive-hedging algorithm must be carefully selected, or alternatives for the coordination of the dual variables should be developed to obtain an advantage of the decomposition. In Atakan and Sen (2018) (and the references therein), several approaches for the coordination of dual variables are described, one of the most broadly used the one presented in Rockafellar and Wets (1991). In this approach, the authors addressed the issue of coordinating the dual variables using projection and proximal point algorithms.

Robust approach for the real-time operation of power systems

The uncertainty modeling method for formulating the unit commitment for the short-term robust operation of power systems was carried out from a finite set composed of 3 elements (Boyd and Vandenberghe, 2004). These elements correspond to the low, medium, and high operating conditions of the system, obtained from the lower and upper historical envelopes for the demand and the non-conventional renewable generation (solar and wind) of energy, and the average value of demand energy and power generation by non-conventional energy sources. Thus, the conditions are defined as:

- Low: lower envelope of the demand and the energy generated by non-conventional energy sources.
- Medium: mean historical value for the demand and the energy generated by the non-conventional energy sources.
- High: upper envelope of the demand and the energy generated by the non-conventional energy sources.

The conditions above are illustrated in figures 3 and 4. These figures correspond to the total renewable generation and total electricity demand, i.e., the sum of the energy produced by each solar and wind power plant and the sum of the electric energy demanded at each load node at a given hour.

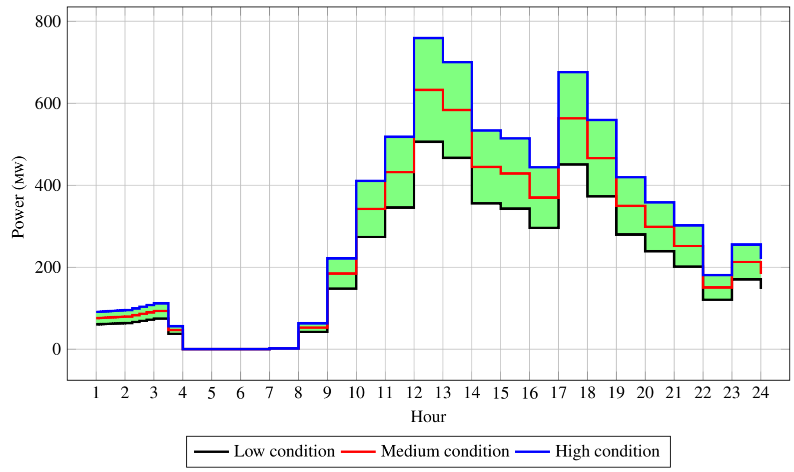

Figure 3. Uncertainty representation/modeling for the non-conventional renewable generation

Figure 4. Uncertainty representation/modeling for the electric energy demand

In general terms, the scenarios/conditions shown in figures 3 and 4 can be assumed as elements of uncertainty set $\mathcal{A} = \{A_1, \ldots, A_k\}$, with $A_1, \ldots, A_k$ each condition considered in the uncertainty representation (in this case low, medium and high conditions, for instance). Then, the robust formulation considering such uncertainty set becomes (Boyd and Vandenberghe, 2004):

$$\min \max_{i=1,\ldots,k} ||A_i x - b|| \tag{64}$$

Whose epigraph form is given by:

$$\begin{aligned} \min \quad & t \\ s.t. \quad & ||A_i x - b|| \leq t, \quad i = 1, \ldots, k \end{aligned} \tag{65}$$

To include the uncertainty presented in Figures 3 and 4 into the unit commitment for the short-term operation of power systems, the rationale for deriving the expression (65) was followed. Consequently, the cost function was replaced by:

$$\min \sum_{t \in T} \sum_{i \in I} \left(h_t \left(\sum_{f \in \mathcal{F}^i} (C_{i,f,t} B_{i,f,t} \beta_{i,f,t}) + \mathrm{NLC}_i (u_{i,t} - u_{i,t}^{syn}) \right) \right.$$
$$\left. + \sum_{j \in \mathcal{J}} \mathrm{SUC}_t^j y_{i,t}^j + \mathrm{SDC}_i z_{i,t} \right) + \varepsilon \tag{66}$$

Since the power balance at every system node must be satisfied in every scenario/condition considered as elements of the uncertainty set $\mathcal{A}$, the power flow equations must be formulated for each. Let every condition considered for the uncertainty be represented by a tuple $(p_{w,t}^{\alpha}, p_{ph,t}^{\alpha}, p_{l,t}^{\alpha}, q_{l,t}^{\alpha})$, with α an index that indicates the combination of conditions that give rise to the specific scenario (e.g., $\alpha = 1$ indicates that the values of all the 3 elements in the tuple come from their upper boundary). Thus, $A_{\alpha} = (p_{w,t}^{\alpha}, p_{ph,t}^{\alpha}, p_{l,t}^{\alpha}, q_{l,t}^{\alpha})$, $\alpha = 1, \ldots, 27$. It is important to remark that in the case of $p_{l,t}^{\alpha}$ and $q_{l,t}^{\alpha})$, their values come from the same boundary, i.e., if the value of α indicates that the value of the active power comes from its corresponding upper boundary, then the value of the reactive power also comes from its corresponding upper boundary. Thereby, the power flow constraints for the robust real-time operation of power systems become:

$$\sqrt{2} G_{n,n} \vartheta_{n,t} + \sum_{\substack{k \in \mathcal{N}^{\mathcal{GEN}} \cup \mathcal{N}^{\mathcal{DEM}} \\ n \neq k}} [G_{k,n} rl_{k,n,t} + B_{k,n} tl_{k,n,t}] = p_{n,t}^{\mathrm{SCH},\alpha}$$
$$\forall n \in \mathcal{N}^{\mathcal{GEN}} \cup \mathcal{N}^{\mathcal{DEM}}, \forall t \in \mathcal{T}, \forall \alpha \in \mathcal{A} \tag{67}$$

$$- \sqrt{2} B_{n,n} \vartheta_{n,t} - \sum_{\substack{k \in \mathcal{N}^{\mathcal{DEM}} \\ n \neq k}} [B_{k,n} rl_{k,n,t} - G_{k,n} tl_{k,n,t}] = q_{n,t}^{\mathrm{SCH},\alpha}$$
$$\forall n \in \mathcal{N}^{\mathcal{DEM}}, \forall t \in \mathcal{T}, \forall \alpha \in \mathcal{A} \tag{68}$$

where $p_{n,t}^{\mathrm{SCH},\alpha} = p_{i,t} + p_{w,t}^{\alpha} + p_{ph,t}^{\alpha} - p_{l,t}^{\alpha} + \varepsilon$, $\forall n \in \mathcal{N}$, $\forall t \in \mathcal{T}$, $\forall i \in \mathcal{I}$, $\forall w \in \mathcal{W}$, $\forall ph \in \mathcal{PH}$, $\forall l \in \mathcal{L}$, $\forall \alpha \in \mathcal{A}$; and $q_{n,t}^{\mathrm{SCH},\alpha} = q_{i,t} - q_{l,t}^{\alpha} + \varepsilon$, $\forall n \in \mathcal{N}$, $\forall t \in \mathcal{T}$, $\forall l \in \mathcal{L}$, $\forall s \in \mathcal{A}$; with ε a slack variable associated with the epigraph of the set $\mathcal{A}$.

In the first instance, for the solution of the resulting optimization problem, and according to the postulation of the problem, it is possible to use solvers associated with linear programming and its variations. However, if quadratic constraints are present within a problem, the computation time is significantly longer. Therefore, alternative solutions have been developed, such as new algorithms rethinking the problem, among others (Ben-Tal, El Ghaoui and Nemirovskiĭ, 2009).

An example of this corresponds to the so-called robust multistage optimization scenarios. They present a finite number of decision variables but with infinite constraints, making it necessary to reframe the problem as deterministic by creating additional variables and constraints (Lorca and Sun, 2017). Within this, techniques such as one-tree

Benders are considered, which correspond to the division of a problem into a pure and linear integer programming exercise to reduce execution times (Murphy, 2013).

From a computational point of view, using uncertainty sets based on budget constraints increases the combinational growth of the number of vertices of the polyhedron concerning the total number of uncertainty parameters. Therefore, techniques such as CCGA (García-Fernández, 2020) and Benders decomposition (Hooker, 2016) have been designed, which are based on an iterative solution of a main or master problem and a subproblem, the latter being corresponding to the worst case scenario (Velloso *et al.*, 2020; Wang *et al.*, 2013).

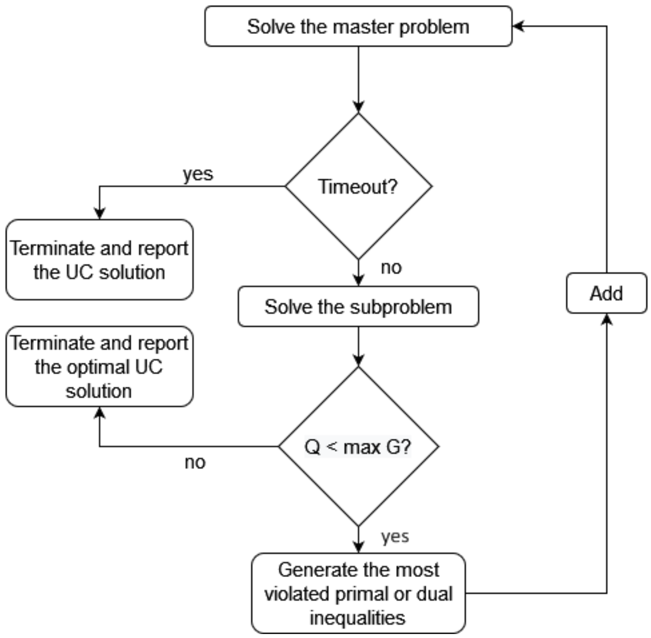

Figure 5. Algorithm used for the solution of the robust unit commitment problem

Source: Wang *et al.* (2013).

In this framework, combinations of methods have also been implemented. An example is presented in Cobos *et al.* (2018) where authors used a combination of CCGA method with lexicographical optimization within the sub-problem to accelerate the finite convergence to optimality. This procedure is illustrated in figure 6. It is worth noticed that, in this approach, the concept of the unpredictability of the dispatch process is introduced. From this concept, the challenges posed by the uncertainty in the dispatch are addressed, specifically for power systems with uncertainty in the generation.

On the other hand, in Zhao and Zeng (2012), an improvement of the cutting plane algorithm was made with a different approach for a robust 2-stage model based on a new validity of inequalities and to achieve the convergence of the objective function, resulting in the following advantages over the Benders dual model:

- This algorithm does not require information from any dual problems.
- It allows linking the decision variables of the first and second stages through a wind energy supply based on scenarios and predictions.

- This method only needs a specific value of wind energy output power in its generation; any point in the uncertainty set can lead to a valid inequality in the master problem.

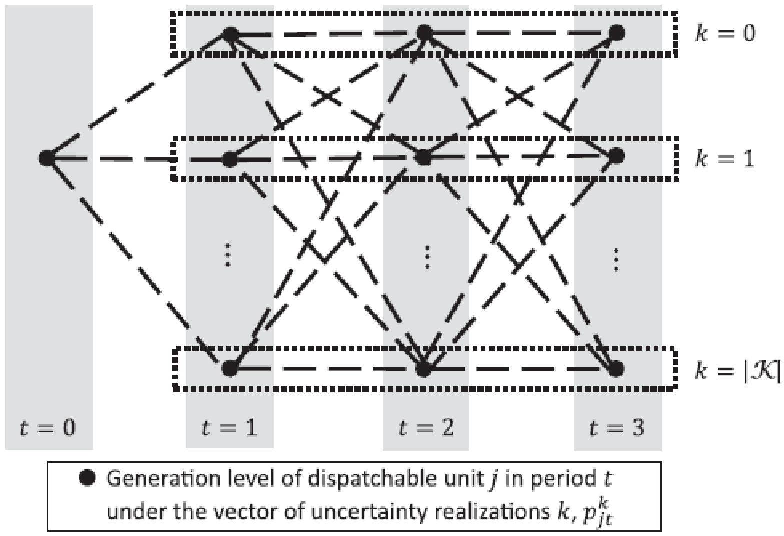

Figure 6. Decision tree considering non-anticipation constraints

Source: Cobos *et al.* (2018).

Simulation results

Stochastic unit commitment

Figure 7 shows the case study used to evaluate the performance of the proposed stochastic unit commitment for the short-term operation of power systems. To solve the optimization problem, both the PH method and the EF method were considered. The Colombian system inspires this case study and corresponds to the areas in which it is divided for its operation and the interconnection between them.

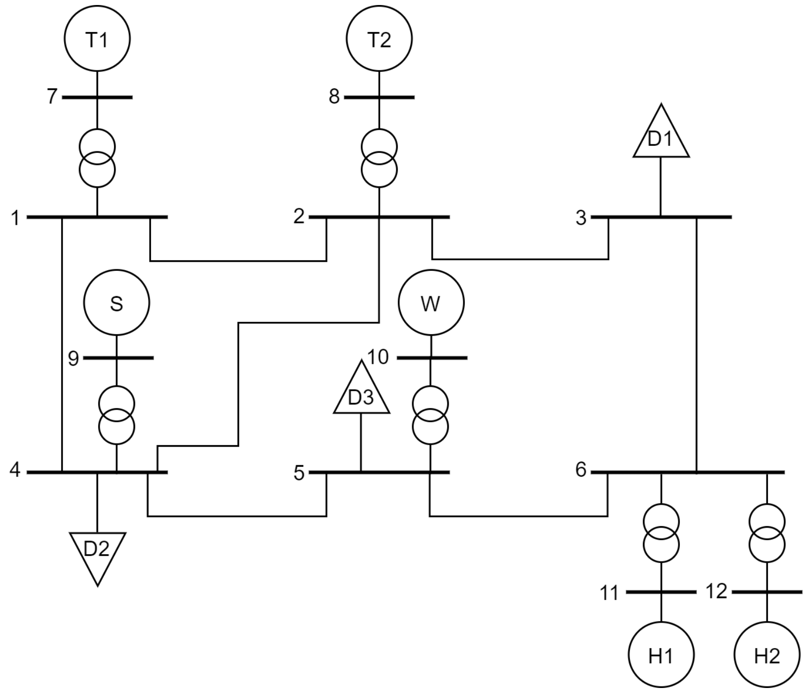

Figure 7. Single line diagram of the system used as test-bench

Table 4 presents the general description of the test system with all its units.

Table 4. Test case description

Number of buses	12
Number of generators	4
Number of wind farms	1
Number of solar plants	1
Number of charges	3
Number of lines	7
Number of periods in the horizon |T|	24
Granularity	1 h
Number of scenarios per period	243

In table 5, on the other hand, the maximum values of each of the generation units are indicated, being the Hydro1 units of a hydroelectric nature and Thermalgas1 of a thermal nature.

Table 5. Technical data of the system generators

Generator	Pmax [MW]	Pmin [MW]	Marginal cost [COP]
(H1) Hydro1	200	0	361000
(H2) Hydro2	22.06	0	362900
(T1) Thermalgas1	100	0	316350
(T2) Thermaloil1	35	0	409146
(S) Solar1	20	0	38000
(W) Wind1	20	0	38000

Finally, the table 6 presents the reference values for constructing transmission line parameters based on the IEEE 9-bus model, which in this case has the same properties and distance of 15 km. The transformer reactance data is also similar.

Table 6. Item values based on the IEEE 9-node model

Parameter	R (pu/m)	X (pu/m)	B (pu/m)
Lines	0.01	0.068	0.176
Transformers	0	0.0586	0

A simulation was carried out with 243 uniformly distributed scenarios. The results were arranged in tables to analyze the distributions of the variables of interest. Figures 8 and 9 present the box-and-whisker plots of non-conventional renewable generation and demand for each hour of the day according to the scenarios included in this analysis. As can be seen, the maximum variation occurs in the hours of greatest availability of non-conventional energy, i.e., of solar generation during midday hours and of wind generation at the end of the afternoon.

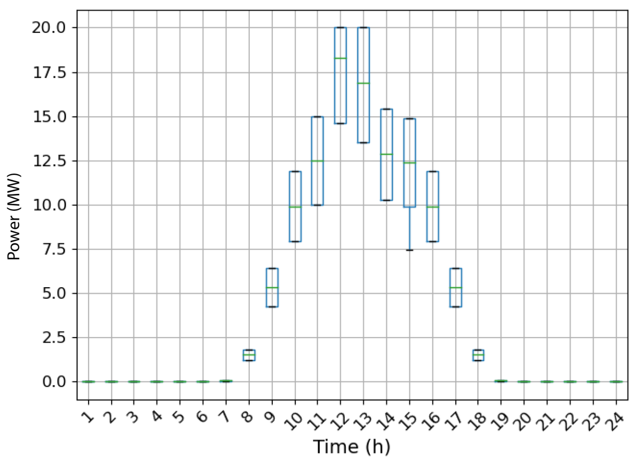

(a) Boxplot for the solar generation

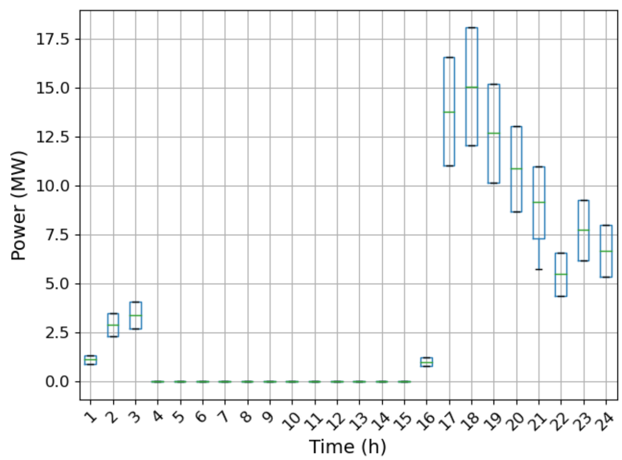

(b) Boxplot for the wind generation

Figure 8. Hourly distribution of the solar and wind generation

Figure 10a shows the behavior of the energy injected by each generation unit in each of the scenarios. According to the net energy demand, the scenarios are organized from lowest to highest in this simulation. As can be seen, hydroelectric power plants cover the additional demand while the thermal power plant maintains its generation more or less constant. To obtain these results, minimum energy injected into the network of 2420 MWh/day was established, with an average of 3120 MWh/day, and a maximum of 3580 MWh/day. Bearing this in mind, non-conventional renewable generation represents 6.8 % to 7.8 % of demand.

As a complement, figure 10b shows the behavior of the reserves in each of the scenarios per generation unit. Due to the use of hydraulic generation plants, the gas-fired thermal generator is the generation unit that has the most energy available for reserves, followed by the diesel-fired thermal, which is the one that covers the non-spinning tertiary reserve requirements. In addition, it is observed that hydroelectric plants are used to provide flexibility to the system since they have a greater load intake and shedding capacity. Thus, these generation plants contribute mainly to primary reserves in abrupt variations of non-conventional renewable generation or demand. It is worth emphasizing that, in those scenarios where the D3 demand is higher, the largest reserve allocations are obtained, higher than 1400 MWh/day. This is more evident in scenarios where non-conventional renewable generation is also high.

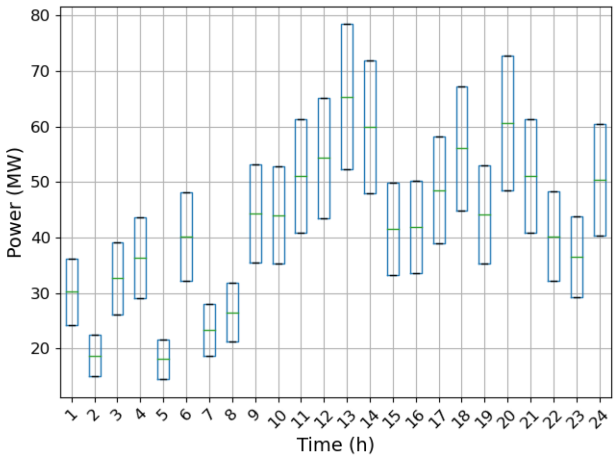

(a) Boxplot for the demand D1

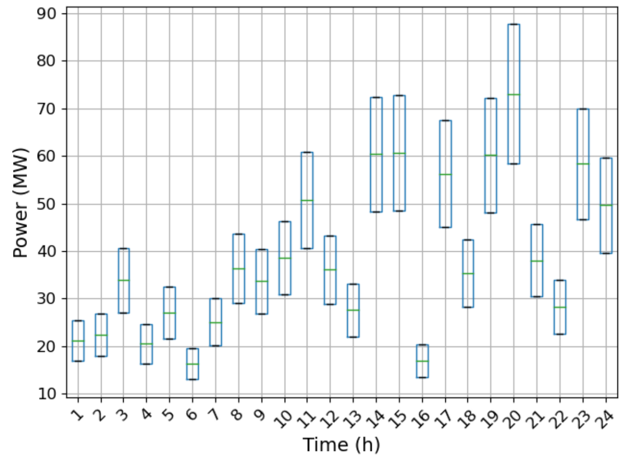

(b) Boxplot for the demand D2

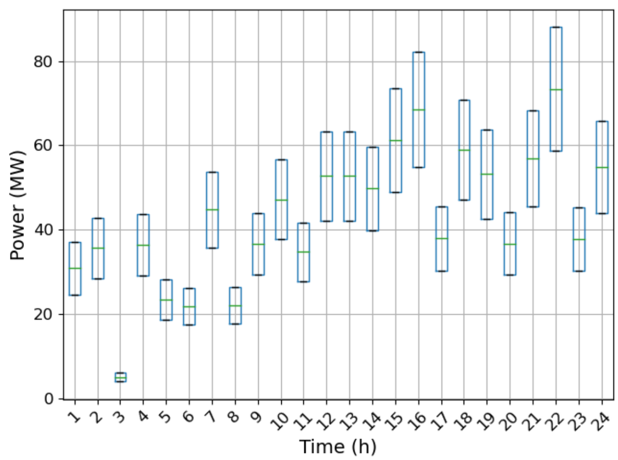

(c) MWplot for the demand D3

Figure 9. Hourly distribution of the demand at each load node

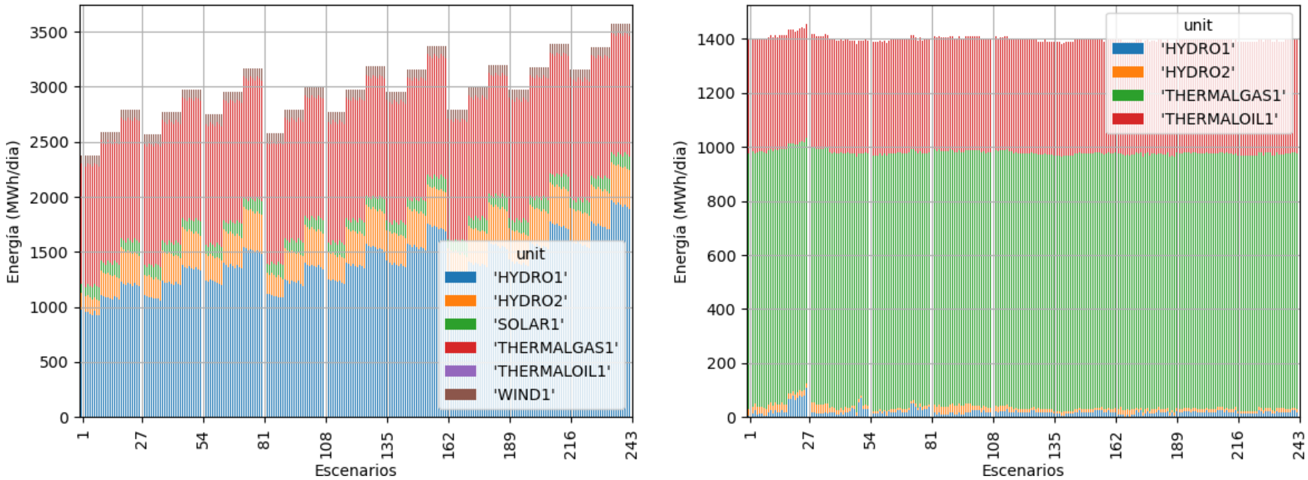

(a) Energy injected by each generation unit as a function of the scenarios included in the analysis

(b) Reserves allocation as a function of the scenarios considered in the analysis

Figure 10. Distribution of the dispatch and reserves allocation in the generation units as a function of the scenarios considered in the analysis

The distribution of the allocation of reserves throughout the day for each generation unit is presented in figure 11. The intensity of the color of the marker accounts for the number of times each assignment is repeated (the more intense, in more scenarios of the 243, that quantity and type of reservation were assigned). Figure 11 clearly shows that the hydraulic generation units participate mainly in the primary and secondary rising reserves and that participation does not present a regular pattern. On the contrary, the gas-fired thermal plant has a clear pattern of participation in the upstream secondary reserve, determined by its load intake/shedding capacity. Finally, it can be seen that the diesel generation plant only participates in the non-spinning tertiary reserve.

Finally, it was analyzed how the operation phases vary: desynchronization, dispatch, soak, and synchronization of the generation units depending on the scenarios, especially the hydraulic units, which are the ones that present a more variable behavior given their flexibility. Figure 12a shows the operating stage in which hydroelectric generation unit 1 is found. In this figure, it is evident that at hours 1, 15, 16, 20, and 21, the unit is with high probability in a desynchronized state, while at hours 4, 7, 9, 14, 18, 19, and 24, this generation unit is, with a high probability, in the synchronization stage. The other stages are more or less uniform, depending on the scenarios. Figure 12b presents the distribution of the operating stages of hydroelectric generation unit 2. In this case, the desynchronization stage has a greater probability of occurring at hours 7, 8, 14, 15, 18, 19, 21, and 23, while at hours 1, 4, and 5, this generation unit is, with a high probability, in the dispatchable stage.

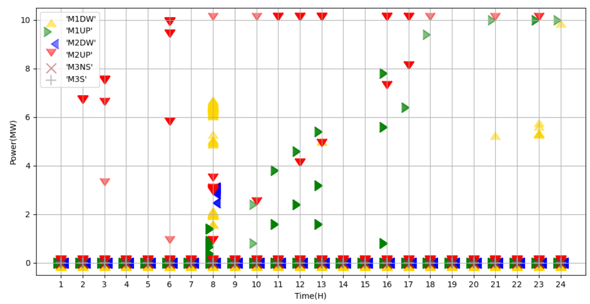

(a) Reserves allocated in the hydroelectric power plant 1

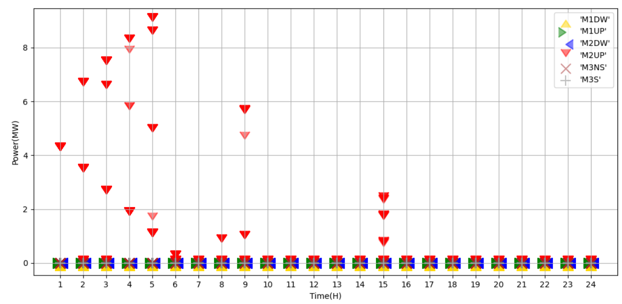

(b) Reserves allocated in the hydroelectric power plant 2

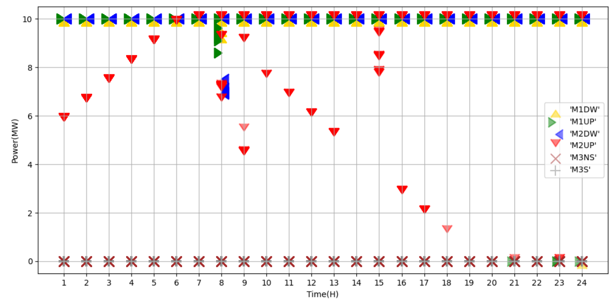

(c) Reserves allocated in the gas-fired thermal power plant

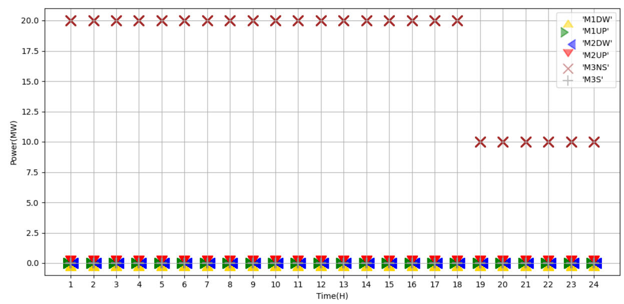

(d) Reserves allocated in the diesel-fired thermal power plant

Figure 11. Reserves allocation throughout the day for each generation technology

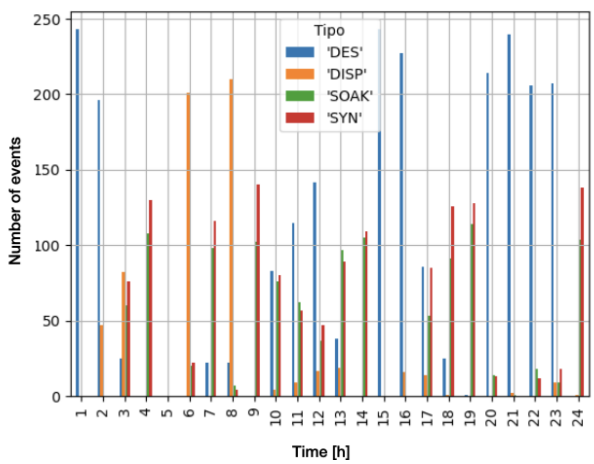

(a) Hydoelectric 1 phase assignment

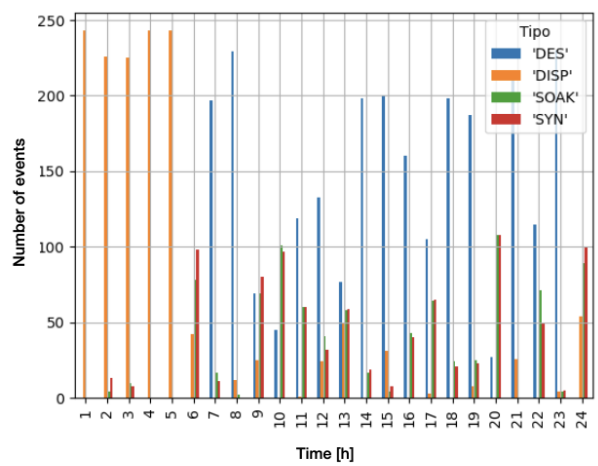

(b) Hydoelectric 2 phase assignment

Figure 12. Results of phase assignment according to the type of event in hydroelectric plants

Robust unit commitment

To evaluate the performance of the robust unit commitment strategy for the short-term operation of power systems, the 39-node IEEE system was considered. The table 7 shows the main analysis parameters of the implemented model, given by a set of transmission lines and transformers.

Table 7. Test case description

Number of buses	39
Number of traditional generators	8
Number of wind farms	1
Number of solar plants	1
Number of charges	19
Number of lines	34
Number of transformers	12
Number of periods in the horizon |T|	24 and 39
Granularity	1 h - 5 to 30 min

In turn, the table 8 shows the main operating values of each generation plant, comprised of the power limits, up and down ramps, and definition of AGC operation.

Table 8. Generation parameters

Plant	P_{max} (MW)	P_{min} (MW)	P_{max} agc (MW)	P_{min} agc (MW)	Ramp Down (MW/h)	Ramp Rise (MW/h)	Q_{max} (Mvar)	Q_{min} (Mvar)
Hydro (G01)	1000	80	800	300	250	250	300	-150
Hydro (G02)	600	222	500	222	300	300	300	-150
Hydro (G03)	730	500	0	0	200	200	300	-150
Thermal (G04)	791	200	700	200	105	105	250	-150
Thermal (G05)	455	224	0	0	33	33	167	-150
Wind (G06)	687	0	0	0	687	687	0*	0*
Thermal (G07)	791	200	700	200	105	105	240	-150
Thermal (G08)	455	224	0	0	33	33	250	-150
Solar (G09)	865	0	0	0	865	865	0*	0*
Hydro (G10)	1200	300	900	300	250	250	300	-150

In the table 9, the operating costs of the system are presented following the modeling of Bakirtzis *et al.* (2014b), given mainly by the marginal price range (given in a distribution of 4 steps) associated with the power of output of each generator in the dispatch process.

Tables 10 and 11 show the reserve limits per resource and the minimum power data to be assigned per type of reserve, respectively.

Table 9. System operating costs

Plant	No load cost (COP/h)	Shutdown cost (COP)	Startup cost in Hot (COP)	Start-up cost in warm (COP)	Cold start cost (COP)	Marginal Cost Range (COP/MWh)
Hydro (G01)	0	0	0	0	0	361000-364800
Hydro (G02)	0	0	0	0	0	362900-364610
Hydro (G03)	0	0	0	0	0	361000-364800
Thermal (G04)	7197.2	76000	177080	243226.6	331424.6	316350-570000
Thermal (G05)	12794	38000	60845.6	94361.6	161393.6	409146-437000
Wind (G06)	0	0	0	0	0	38000-76000
Thermal (G07)	7197.2	76000	177080	243226.6	331424.6	316350-570000
Thermal (G08)	12794	38000	60845.6	94361.6	161393.6	409146-437000
Solar (G09)	0	0	0	0	0	38000-76000
Hydro (G10)	0	0	0	0	0	361000-364800

Table 10. Reserve allocation limits per plant

Generator	M1UP	M1DW	M2UP	M2DW	M3S	M3NS
Hydro (G01)	100	100	100	100	100	100
Hydro (G02)	100	100	100	100	100	100
Hydro (G03)	100	100	100	100	100	100
Thermal (G04)	100	100	100	100	100	100
Thermal (G05)	100	100	100	100	100	100
Wind (G06)	100	100	100	100	100	100
Thermal (G07)	100	100	100	100	100	100
Thermal (G08)	100	100	100	100	100	100
Solar (G09)	100	100	100	100	100	100
Hydro (G10)	100	100	100	100	100	100

Table 11. Minimum system reserve requirements

	M1UP	M1DW	M2UP	M2DW	M3S	M3NS
Reserve	300	300	300	300	300	300

Figure 13 shows the output power assigned to Hydroelectric G01 for the 4 reference cases: deterministic hourly and intrahourly, and robust hourly and intrahourly. The trend between scenarios was identified as similar, with a maximum difference between the hourly robust scenario and the others of 180 MW. This is due to the reassignment of plants due to the effect of intrahour intervals, which change the behavior of hydroelectric plants, as these are the ones that present a faster response than thermal ones. Within this, in the hourly robust case, a redistribution of resource allocation is shown between hours 9 and 13 due to the adaptation of the system to uncertainty and the use of other hydroelectric and thermal plants. This is similarly presented at hour 17.

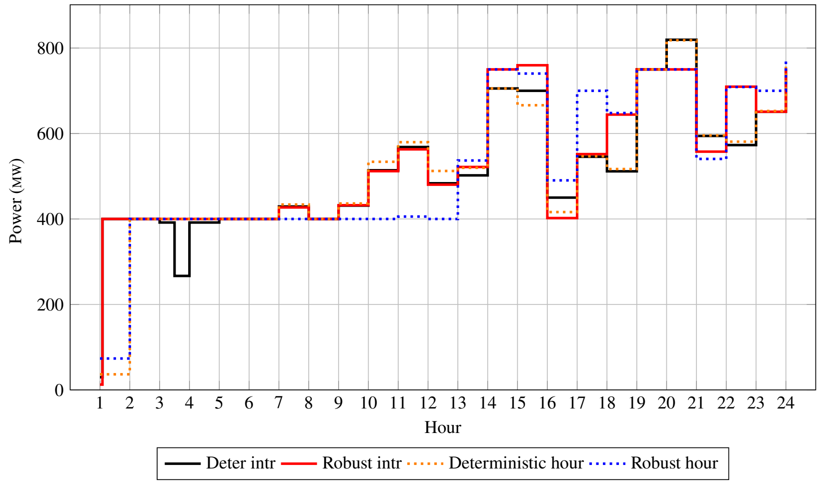

Figure 13. Output power of the hydroelectric generator G01 for each case of analysis

However, in the case of thermal plants, there is a marked difference in dispatch as summarized in figure 14 at night, with a maximum value of 575 MW at hour 20. This phenomenon occurs due to the effects of uncertainty in these hours, where thermal plants increase their dispatch due to coverage of demand and renewable generation.

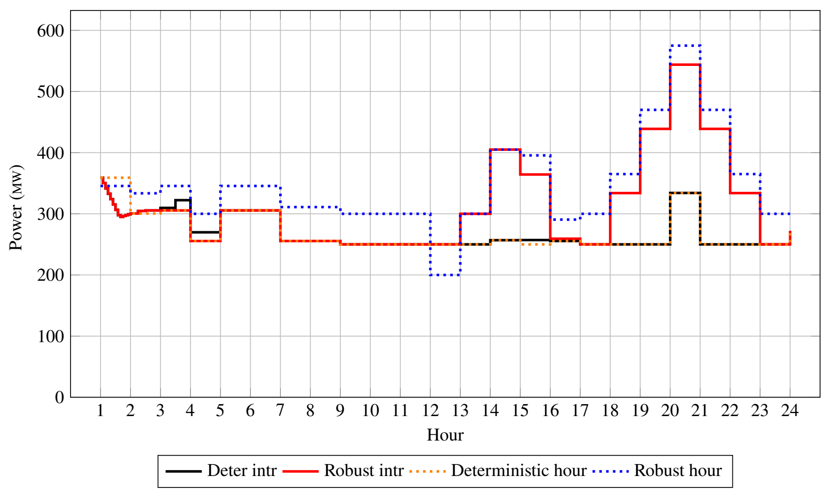

Figure 14. Power output of the thermal plant G04 for each case of analysis

In the same way, a redistribution of the allocation of thermal and hydroelectric generation sources related to the percentage of substitution of the demand was presented. Specifically, figure 15 shows the power allocation percentage for hydroelectric plants, with a main difference in the hourly deterministic model due to the operation in the first hour of the dispatch in which it is decided to less use of water resources even though all the scenarios have the same initial conditions.

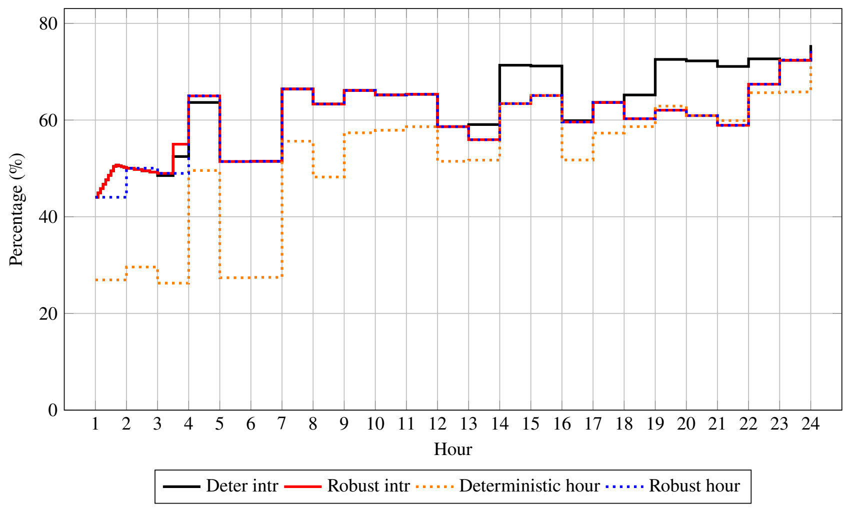

Figure 15. Percentage of participation of hydroelectric generation plants

This phenomenon was identified in the figure 16 for the hourly case, with a greater contribution from the thermal plants in the first hours of the diagnosis. For the night intervals, the robust models showed an increase in the participation of this plant, associated with the fulfillment of the criteria of the constructed cases.

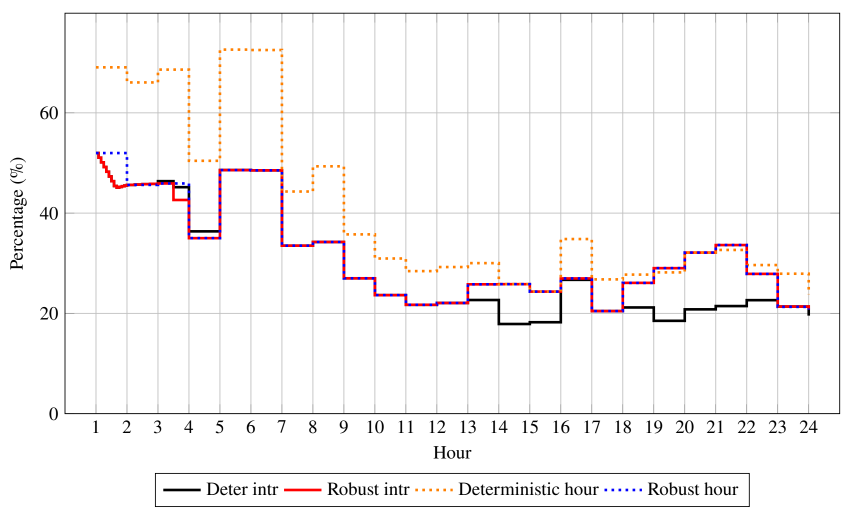

Figure 16. Percentage of participation of thermal generation plants

In addition to the differences already mentioned in the dispatch of the units depending on the case analyzed, differences were found in the assignment of the phases that the units must follow before their connection/disconnection from the system. For example, it was identified that for hydroelectric plants, the assignment to the soak and desynchronization stages is concentrated in the first 3 hours of the day, with another change at hour 12, as can be seen in figures 17 and 18.

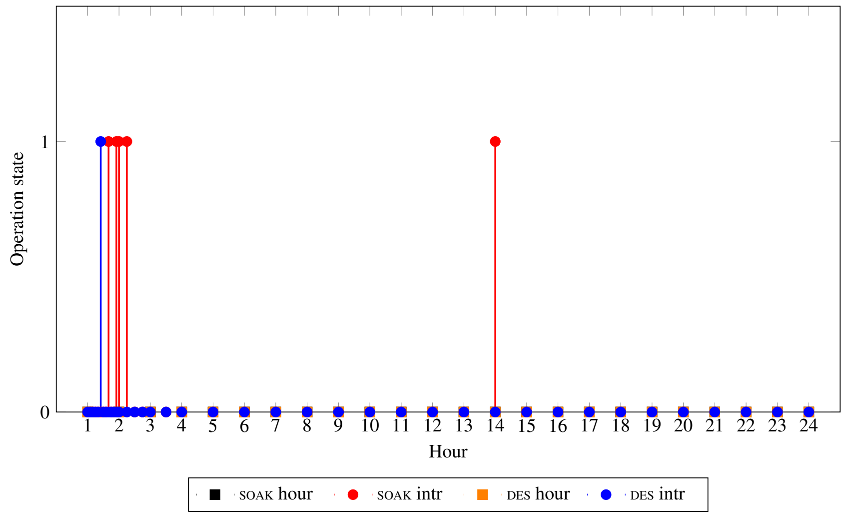

Figure 17. Assignment of soak and desynchronization stages in the deterministic case for hydroelectric power plant G10

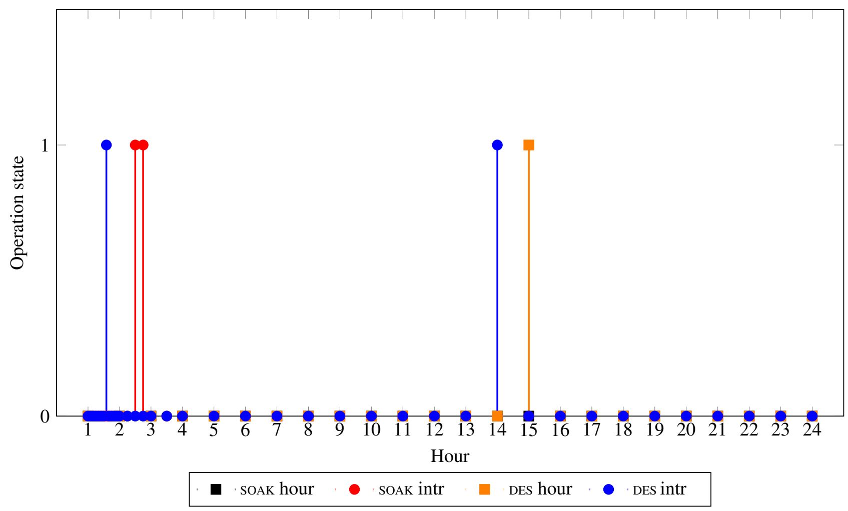

Figure 18. Assignment of soak and desynchronization stages in the robust case for hydroelectric power plant G10

In turn, the allocation was recorded in the same hours for both the deterministic and the robust models while the allocation was modified in intrahour intervals. This is because hydroelectric plants are assigned to the dispatchable stage in most of the 24 hours of analysis. In fact, the power corresponding to the soak phase is assigned in its entirety to the hydroelectric plants as shown in figure 19, with the recording of different values between each type of case analyzed and bounded by the output power and the use of reserves, in which the latter represents the flexibility of these plants.

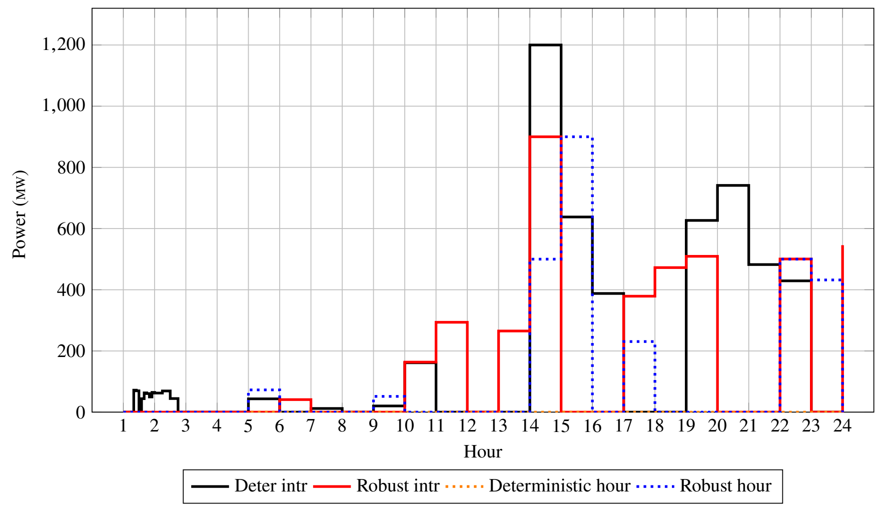

Figure 19. Generation of the G10 hydroelectric plant in the soak stage

Regarding the reserves, the different patterns associated with the allocation of these resources were identified and referenced by the categories primary (upper and lower), secondary (upper and lower), and tertiary (rotating and non-rotating) (Bakirtzis *et al.*, 2014b). For the allocation of reserves, the following parameters were considered:

- Maximum power of each hydroelectric and thermal generation plant.
- Assignment of the plants to the different system operation stages and the associated power value.
- Minimum and maximum power limits dedicated to the AGC process.

Specifically, throughout the analysis interval, a plant must be assigned to the dispatchable phase to deliver primary or tertiary spinning reserve. In turn, for secondary reserves, it is required that the plant be simultaneously operating in the dispatchable stage and on the list of units that can provide the AGC service. In the case of the non-spinning tertiary reserve, it is required that it be a plant that is not operating in any of the stages: soak, synchronization, or dispatchable.

Regarding the total value of reserves, it was proposed to assign a minimum requirement value for each type of generation plant, measured in MW, which in this analysis corresponds to a value of 300 MW. However, for tertiary reserves, a sum is made between the revolving and non-revolving reserves to meet the minimum value. These conditions are summarized in the following equations:

$$\sum_{i \in \mathcal{I}} r_{i,t}^{m} \geq R_t^{sys,m} \quad \forall t \in \mathcal{T}, m \in \{1^+, 1^-, 2^+, 2^-\} \tag{69}$$

$$\sum_{i \in \mathcal{I}} r_{i,t}^{3N} + \sum_{i \in \mathcal{I}} r_{i,t}^{3NS} \geq R_t^{sys,3} \quad \forall t \in \mathcal{T} \tag{70}$$

Figure 20 shows the allocation of the lower primary reserve for the G04 thermal plant throughout the 24 hours of analysis, where it is evident that for the robust hourly model, there are allocation peaks of 100 MW, which is the maximum capacity that this plant can provide and that is related to the distribution of total dispatched power assigned to the thermal plants in figure 16. The effect of considering hourly and intrahourly intervals can be seen in the first 3 hours of the day since there is a progressive change from 60 to 50 MW during the 5-minute intervals. This is also related to the maximum capacity the plant can deliver, adding the dispatch with the contribution of the other types of reserves.

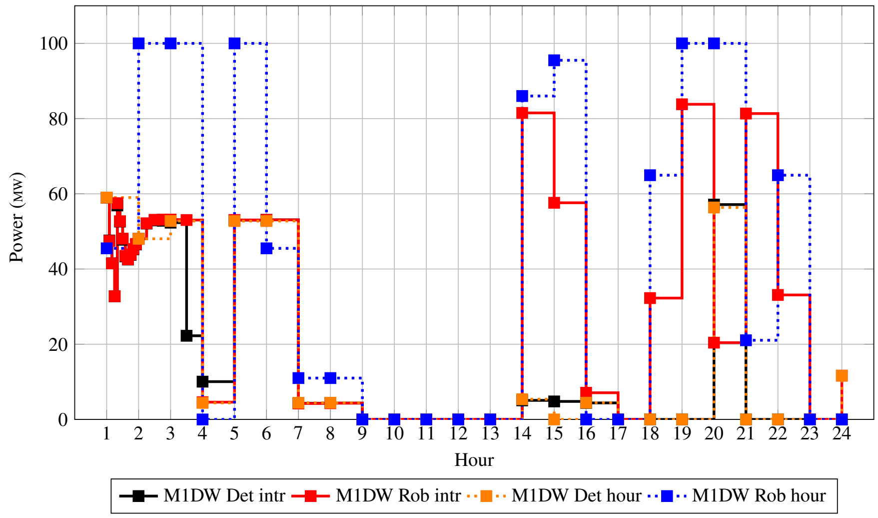

Figure 20. Primary reserve behavior (lower) for the thermal generator G04

This phenomenon is evidenced similarly in figure 21 since in this thermal plant, an assignment of 100 MW is made in most hours in the hourly case with uncertainty, but this changes for the other 3 cases where the intervals together with the inclusion of uncertainty reduce the contribution. On the other hand, in the intervals where a value of 0 was recorded, they correspond to changes to satisfy the maximum power that this generator can deliver.

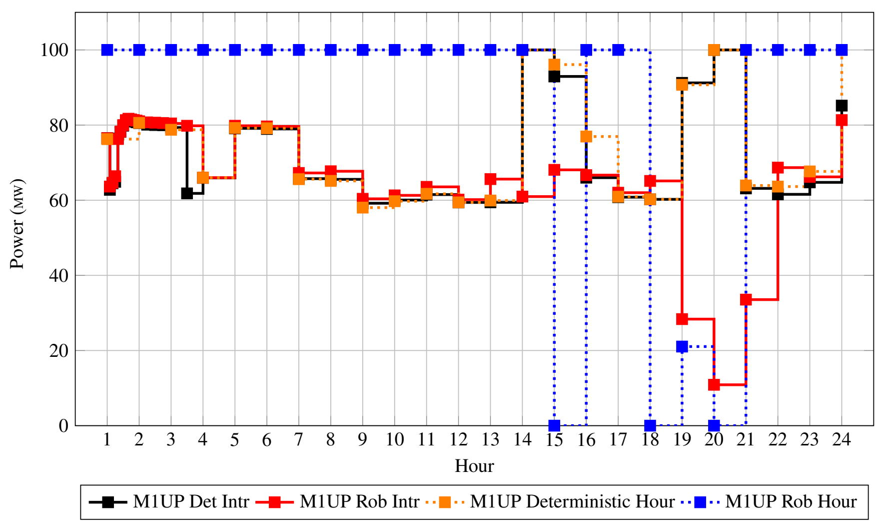

Figure 21. Primary reserve behavior (upper) for the thermal generator G04

In the case of hydroelectric plants, both primary and secondary reserves are assigned since these plants were enabled to provide this service. Specifically, the lower AGC reservation for exchange G01 is presented in figure 22, and figure 23 shows the upper secondary. It is worth noting that in the intrahourly case, regardless of the uncertainty, there are hours of no-reserve allocation since the plant does not meet the conditions for having a secondary reserve allocation. This is clearer in the intrahourly case due to the granularity of its solution.

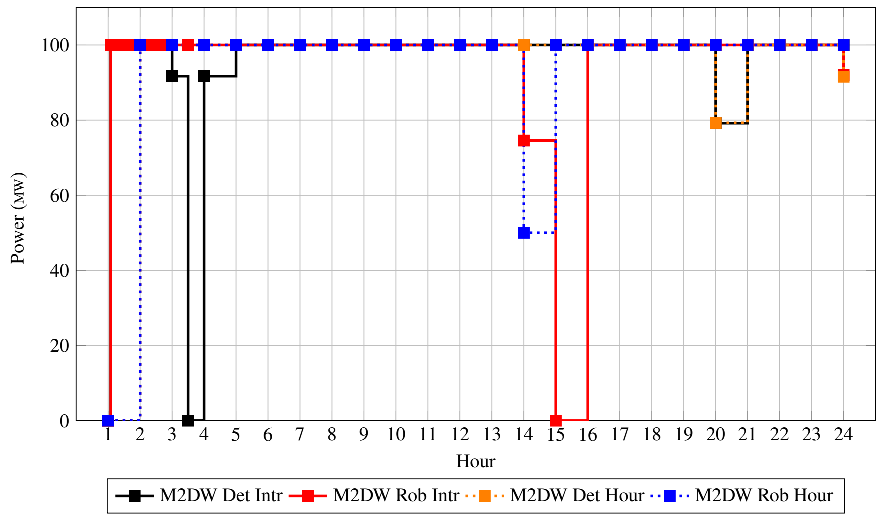

Figure 22. Secondary reserve behavior (lower) for the hydroelectric power plant G01

Figure 24 shows the assignment of the spinning tertiary reserve for the thermal plant G08. As can be seen, between hours 3 and 9, no-rotating power is assigned to this generation unit, while in the last 5 hours of the day, there is a redistribution of the contribution of this type of reserve, which is more evident in intrahour cases.

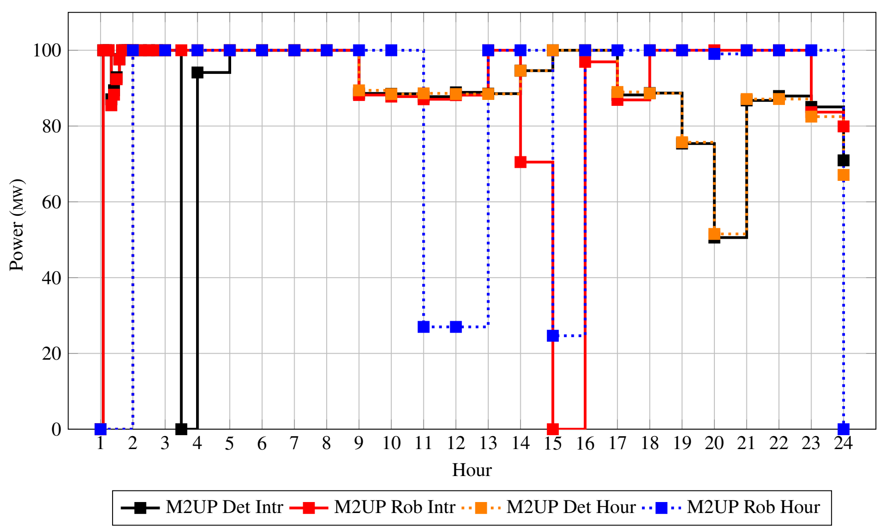

Figure 23. Secondary reserve behavior (upper) for the hydraulic generator G01

Figures 25 and 26 show the total reserve assigned to the hydraulic and thermal generation units, respectively. These figures show that for all cases, the contribution of reserves fluctuates between 400 and 1000 MW for hydroelectric plants and corresponds to primary and secondary reserves. In addition, it is observed that the reserves assigned to thermal plants exhibit a behavior contrary to that of hydraulic plants. This is due to thermal generation plants' inflexibilities, manifested mainly in their load intake rates and the ability to change the operating point.

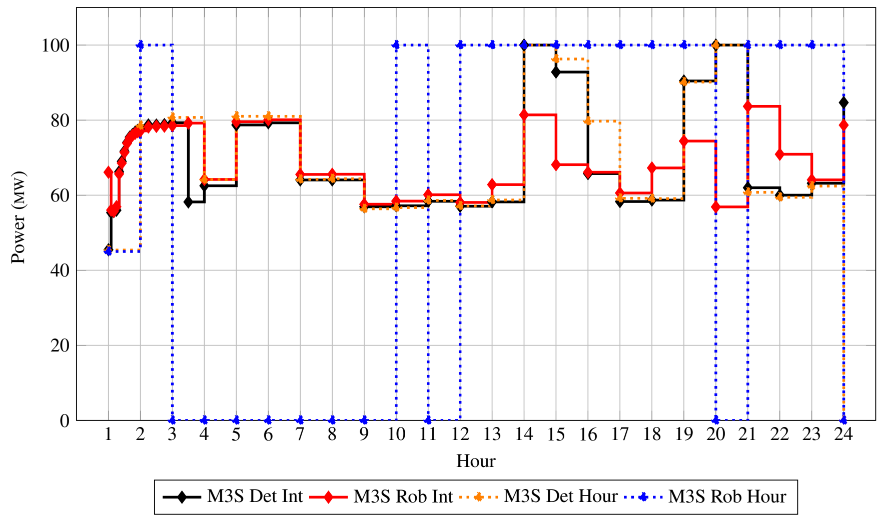

Figure 24. Tertiary reserves behavior for the thermal unit G08

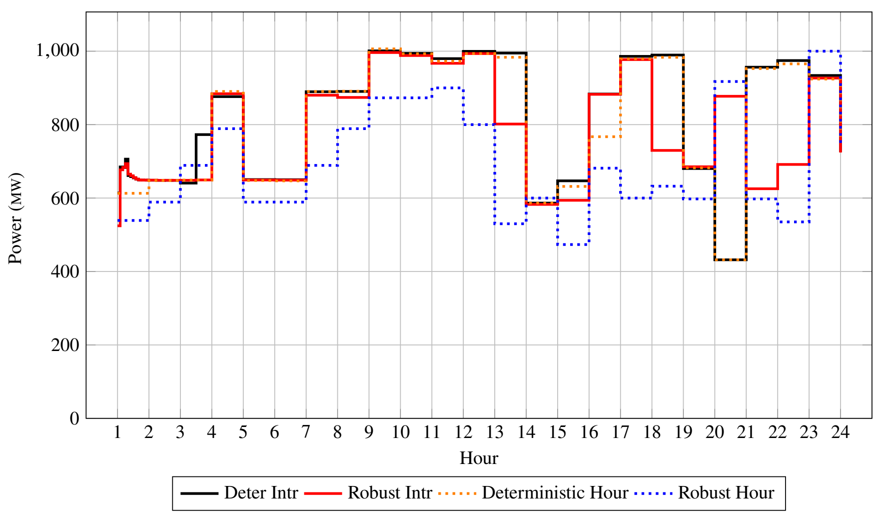

Figure 25. Total amount of reserves allocated in the hydroelectric power plants

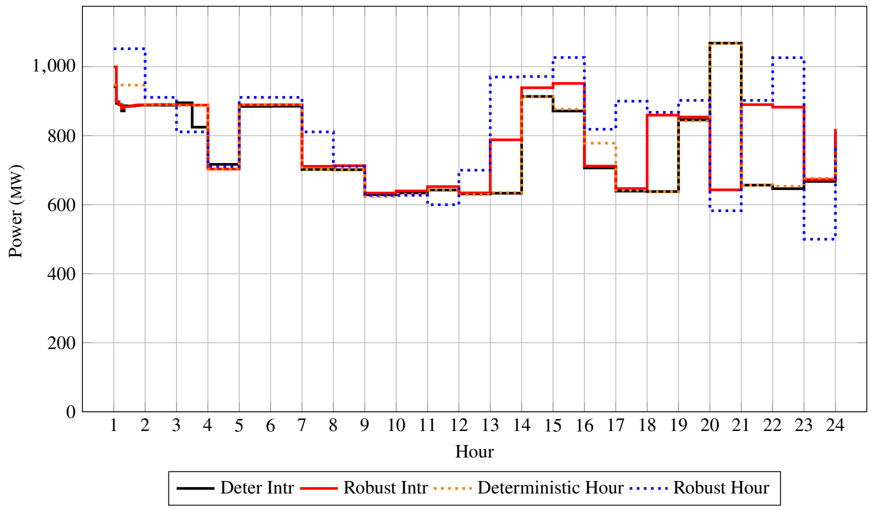

Figure 26. Total amount of reserves allocated in the thermal power plants

Finally, the data were summarized in daily consolidated data to further compare the performance of the methods. In table 12, it was identified, for example, that the total cost of operating the system with the robust models is higher than the deterministic ones by 88 MCOP for the hourly case and 87 MCOP for the intrahour case.

Associated with this point, it was identified that the difference in the total cost of dispatch between hourly and intrahourly cases is less than 15 MCOP. This allows us to conclude that there is no apparent difference between methods under the conditions studied in this chapter. However, the resolution of the solution to the unit commitment problem has important effects on the behavior of the other analysis variables, as presented throughout this section.

Table 12. Total costs of operation and daily energy dispatched by type of resource

Model	Total cost (MCOP)	Output hydroelectric (MWh)	Output thermal (MWh)	Output renewables (MWh)
Deterministic time	23329	46210	18324	6193
Deterministic intraclockwise	23315	46029	18453	6209
Robust time	23417	43846	20689	6193
Robust intraclockwise	23402	43701	20781	6209

This is more evident in the energy dispatched from hydroelectric plants, which in the robust cases (hourly and intrahourly) is lower by 2347 MWh on average. However, the allocation of reserves is done similarly regardless of the case analyzed (see table 13, with some insignificant differences in the hourly robust case, which presents a slight difference in the total assigned reserves.

Table 13. Daily reserve energy per resource and percentage of total

Model	Reserve hydroelectric (MWh)	Reserves thermal (MWh)	Participation hydro (%)	Thermal share (%)
Deterministic time	19479	18268	51.60	48.40
Deterministic intraclockwise	19590	18297	51.71	48.29
Robust time	16623	19628	45.85	54.15
Robust intraclockwise	18695	18996	49.60	50.40

References

An, Y., & Zeng, B. (2015). Exploring the Modeling Capacity of Two-Stage Robust Optimization: Variants of Robust Unit Commitment Model, *IEEE Transactions on Power Systems*, *30*(1), pp. 109-122. DOI: 10.1109/TPWRS.2014.2320880.

Atakan, S., & Sen, S. (2018). A progressive hedging based branch-and-bound algorithm for mixed-integer stochastic programs, *Computational Management Science 15*(3), pp. 501-540.

Babazadeh, R., & Torabi, S. (2018). An adjusted robust optimization method to an integrated production-distribution planning problem in closed-loop supply chains under uncertainty, *International Journal of Information and Management Sciences*, *29*, pp. 1-33.

Bakirtzis, E. A., Biskas, P. N., Labridis, D. P., & Bakirtzis, A. G. (2014a). Multiple time resolution unit commitment for short-term operations scheduling under high renewable penetration, *IEEE Transactions on Power Systems*, *29*(1), pp. 149-159. DOI: 10.1109/TPWRS.2013.2278215.

Bakirtzis, E. A., Biskas, P. N., Labridis, D. P., & Bakirtzis, A. G. (2014b). Multiple time resolution unit commitment for short-term operations scheduling under high renewable penetration, *IEEE Transactions on Power Systems*, *29*(1), pp. 149-159. DOI: 10.1109/TPWRS.2013.2278215.

Ben-Tal, A., El Ghaoui, L., & Nemirovskiĭ, A. S. (2009). *Robust optimization*, Princeton University Press, Princeton. ISBN: 978-0-691-14368-2.

Birge, J. R., & Dempstert, M. (1996). Stochastic programming approaches to stochastic scheduling, *Journal of Global Optimization*, *9*(3), pp. 417-451.

Boyd, S., & Vandenberghe, L. (2004). *Convex Optimization*, 7 edn, Cambridge University Press, New York.

Bynum, M. L., Hackebeil, G. A., Hart, W. E., Laird, C. D., Nicholson, B. L., Siirola, J. D., Watson, J.-P., & Woodruff, D. L. (2021). *Pyomo-optimization modeling in python*, vol. 67, 3 edn, Springer Science & Business Media.